energies

MDPI

Article

Numerical Investigation on Mechanism of Swirling Flow of the Prefilming Air-Blast Fuel Injector

Cheng Cao [1,2], Yaping Gao [1,3], Shaolin Wang [1,2,*], Fuqiang Liu [1,2], Cunxi Liu [1,2,*], Yong Mu [1,2], Deqing Mei [3] and Gang Xu [1,2]

1 Laboratory of Light-Duty Gas-Turbine, Institute of Engineering Thermophysics, Chinese Academy of Sciences, Beijing 100190, China
2 School of Aeronautics and Astronautics, University of Chinese Academy of Sciences, Beijing 100049, China
3 School of Automotive and Traffic Engineering, Jiangsu University, Zhenjiang 212013, China
* Correspondence: wangshaolin@iet.cn (S.W.); liucunxi@iet.cn (C.L.)

Abstract: Prefilming air-blast atomizers are widely used in modern gas turbine combustors. Due to insufficient awareness of the coupling mechanism of multi-stage swirling flow in gas turbines, there is a lack of effective methods for flow field optimization in combustor. In this study, the effect of some critical parameters on the flow field of a prefilming air-blast atomizer was analyzed with CFD. The parameters include the angle and number of the first swirler blades, the angle of the second swirler blades and the angle of sleeve. Furthermore, the coupling mechanism of two-stage swirling airflows of prefilming air-blast atomizer was discussed. Moreover, the influence of the interaction between two-stage counter swirling airflows on the characteristics of flow field was explained. The results show that with the increase in SN_i, the axial length of the primary recirculation zone decreased, while the radial width increased. The starting position of primary recirculation zone (PRZ) moves forward with the increase in SN_o. Reducing the sleeve angle β helps to form the primary recirculation zone. The results indicate that it is the transition of tangential velocity of airflow to radial velocity that promotes the formation of the PRZ. These results provide theoretical support for optimization of the flow field in swirl combustor.

Keywords: pre-filming air-blast atomizer; two-stage swirl; structural parameters; flow filed; numerical simulation

check for updates

Citation: Cao, C.; Gao, Y.; Wang, S.; Liu, F.; Liu, C.; Mu, Y.; Mei, D.; Xu, G. Numerical Investigation on Mechanism of Swirling Flow of the Prefilming Air-Blast Fuel Injector. *Energies* **2023**, *16*, 650. https://doi.org/10.3390/en16020650

Academic Editors: Changzhao Jiang, Xiao Ma and Yanfei Li

Received: 4 December 2022
Revised: 26 December 2022
Accepted: 29 December 2022
Published: 5 January 2023

1. Introduction

The combustor is one of the major components of aero-engines. The key target of advanced aero-engine research and development is to achieve high efficiency combustion by reasonably organizing fuel-air mixing and optimizing the matching of flow filed with combustor [1–3]. In the combustion system, the atomizer not only plays the role of promoting fuel atomization, but also helps to mix the fuel and air. The prefilming air-blast atomizer is widely used in most modern aero-engines because of some great advantages, such as high atomization quality, large fuel regulation ratio and insensitivity to fuel supply pressure [4].

Based on some newly developed technologies in the field of laser technology, spectral technology and data image processing technology, etc., optical diagnostic technology, as a new spray measurement method, has been widely applied to analyze the mechanism and characteristics of spray and swirling flow in spray combustion process. With this technology, some critical characteristics of combustor (such as the multi-swirl flow field, spray characteristics, concentration of chemical components and flame structure, etc.) have been obtained. Durbin [5] et al. designed a unique step swirl combustor to investigate the impact of key parameters on the flow filed. It was found that the flame length decreased with the increase in the blade angle of outer-stage swirler and the decrease in inner-stage air velocity. Moreover, the lean blowout limitation was improved with the swirl intensity of outer-stage swirler. Wang [6] et al. systematically studied the diesel spray characteristics in the near-field and far-field under room and low temperature with optical diagnostic measurement. The results indicated that, compared with room temperature, the increasing of fuel viscosity under low temperature resulted in less injected fuel, leading to a smaller spray area and poor spray quality. The effect of relative flow orientation between inner and outer-stage swirling air on flow topology with a prefilming air atomizer was approached by Kumar [7] et al. It was found that, as the relative flow orientation switched from counter-rotation to co-rotation, the change in radial width of recirculation zone was negligible. Lin [8] et al. explored the influence of flow field topology in swirl combustor on ignition performance. It was found that the low momentum flow area, which was formed by the primary recirculation zone and the corner recirculation zone, could promote the droplet fragmentation through the increase in aerodynamic and turbulent pulsation and effectively improve the fuel atomization, helping to form the core flame and enhance flame propagation.

In the atomization process of prefilming air-blast atmomizer, there are complex transient processes such as swirling air flow, liquid film breakup, droplet transport and fuel/air mixing, etc. However, current experimental methods cannot obtain all the details in the atomization process of the prefilming air-blast atmomizer. Computational Fluid Dynamics (CFD) is one of the effective tools to analyze three-dimensional complex swirling flow, which can make up for the shortage of experimental tools. Thus, CFD method has been widely used in the optimization and design of aero-engine combustor. Davoudzadeh [9] et al. applied the RANS model to explore the flow field characteristics in the axial swirl combustor. The results show that the central circulation region and corner circulation region downstream of the atomizer exit could be predicted by RANS model. Zeng [10] et al. systematically studied the flow dynamics of two-stage counter-rotating swirler using CFD method with the basis of the experiment. The results indicated that with the increasing of confinement ratio, the flow field morphology showed different patterns successively: the axial growth flow pattern of reflux bubble, contraction flow pattern in the middle of reflux bubble and double reflux bubble flow pattern. Ren [11] et al. used the Reynolds-Averaged Navier–Stokes (RANS) and Large Eddy Simulation (LES) models to predict the flow topology and flame characteristics. It was found that altering the relative rotation direction between outer- and inner-stage swirling flow from co-rotation to counter-rotation resulted in a decrease in flame lift-off equivalence ratio. Mongia [12–14] et al. used the k-ε model to couple the thru-the-vane model and further explored unsteady flow characteristics such as vortex shedding, vortex breakdown and the interaction of main vortexes in the flow field. It was found that the high-intensity unsteady flow caused by the interference of the main injector of the secondary swirler was the main reason for the liquid film breakup. Yoshida [15] et al. applied the single-phase numerical simulation method to study the flow field characteristics of the pre-filming air-blast atomizer under different swirl intensities by changing the angles of the guide vane and the air channel ($\alpha = 0°$, 30°, 45° and 50°). The swirler with reverse arrangement changed the vorticity field formed by swirling effect and improved the atomization quality. Under higher ambient pressure and lower fuel flow rate, the main influencing factor of spray morphology was the local circumferential shear strength generated by swirling airflow.

In summary, previous studies of prefilming air-blast atomizer mainly focus on the influence of flow field structure on spray characteristics or ignition performance and mostly explore the flow field under the combined effect of main and pilot stage. However, there is still insufficient understanding of the internal mechanism and evolution process of swirling flow formed by two-stage swirlers of the airblast atomizer. Therefore, this research adopts the CFD method to study the flow field characteristics of prefilming air-blast atomizer under different swirl combinations. The coupling mechanism of two-stage swirling airflows of prefilming air-blast atomizer was analyzed, and the influence of key parameters of two-stage counter-rotational swirlers on the flow field characteristics was interpreted.

2. Method

The two-stage swirler employed in the present study consists of three components: inner swirler, prefilming air-blast atomizer and outer swirler (see Figure 1). As mentioned above, this work mainly focuses on the effects of structural parameters on the flow field. Although fuel injection has a slight impact on the flow filed, this impact is negligible compared to the structural parameters. Thus, the air-blast atomizer model was simplified and had no fuel circuit (as shown in Figure 1), and the flow fields in all cases were analyzed without fuel injection. The inner and outer swirler moved in counter-rotating directions, and the air mass flow ratio of the internal swirler was 40%.

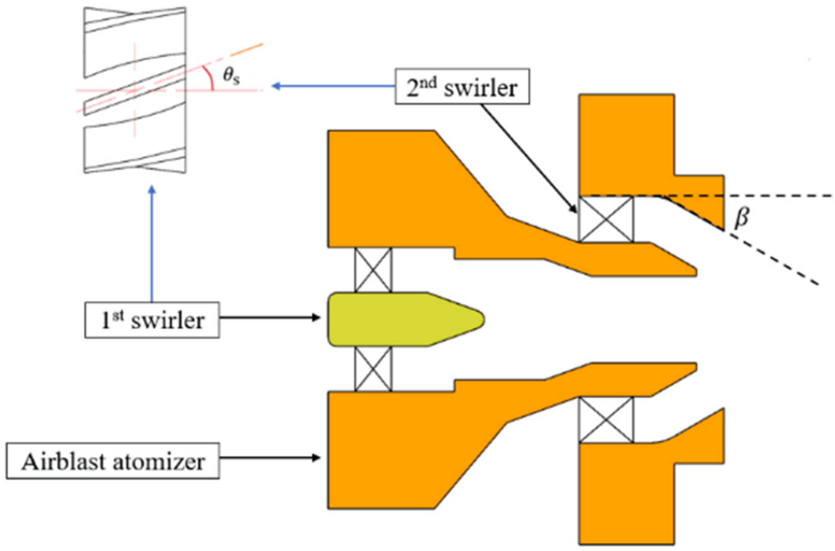

Figure 1. Schematic illustration of the two-stage swirler.

The swirling flow with swirl number greater than 0.6 is usually defined as strong swirling flow, and it is usually used to form a primary recirculation zone [16]. The definition of swirl number is shown in Equation (1) [17]:

$$SN = \frac{G_\varphi}{G_X R_S} \tag{1}$$

where G_φ represents the axial flux of angular momentum; G_X represents the axial flux of axial momentum; R_S represents the outer radius of the swirler. For a straight blade axial swirler with an angle of θ_s, the Equation (1) can be converted to the Equation (2) [17]:

$$SN = \frac{2}{3} tg\theta_S \frac{1 - \left(\frac{r}{R_s}\right)^3}{1 - \left(\frac{r}{R_s}\right)^2} \tag{2}$$

where r represents the inner radius of the swirler.

In order to explore the effect of structural parameters on the flow field, the adopted swirler design schemes are shown in Table 1. The parameters include the blade angle of inner swirler (θ_{s1}), the blade number of inner swirler (n), the blade angle of outer swirl (θ_{s2}), the sleeve angle (β), inner swirl number (SN_i) and outer swirl number (SN_o). Moreover, the '+' represents the clockwise direction from the upstream view.

The numerical simulation of the steady flow field of the two-stage swirl combustor with prefilming air-blast atomizer is carried out in the conditions of normal temperature and pressure. The Coupled algorithm is used in the simulation. The turbulence is modeled using Realizable k-ε model, and pressure inlet and outlet are selected as the boundary conditions. The pressure drop between the inlet and outlet of swirler is 3% and the air mass flow rate is 59.33 kg/h, which is consistent with the experimental condition. The computational domain is discretized using tetrahedral and hexahedral unstructured grids. Moreover, the grid near the swirler blades and air-blast atomizer is refined in order to capture the turbulence and velocity gradients (see Figure 2). The minimum grid size is 0.31 mm and the number of grids is 3311887. In addition, the grid independence of the flow field is verified with the grid numbers of 1 million, 3.31 million and 5.74 million, respectively. The comparison of axial velocities on the central axis is shown in Figure 3. It is found that the axial velocity on the central axis is basically unchanged within the number of grids, ranging from 3,110,000 to 5,740,000. Therefore, a grid number of 3 to 4 million is applied for numerical simulation.

Table 1. Parameters of swirlers.

Schemes	θ_{s1}	n	θ_{s2}	β	SN_i	SN_o
S1	−20°	6	+40°	30°	0.235	0.695
S2	−30°	6	+40°	30°	0.402	0.695
S3	−20°	8	+40°	30°	0.266	0.695
S4	−30°	8	+40°	30°	0.427	0.695
S5	−20°	6	+50°	30°	0.235	0.987
S6	−20°	6	+60°	30°	0.235	1.434
S7	−20°	6	+40°	15°	0.235	0.695

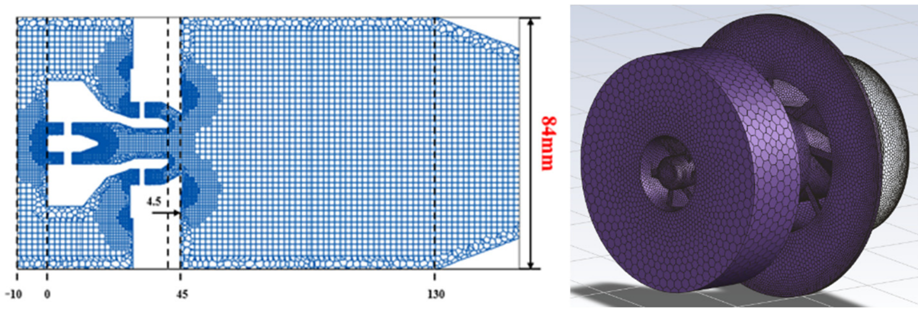

Figure 2. The grids of the combustor with two-stage swirler. (The length of the computational domain is 310 mm, the axial coordinate of the swirler inlet is selected to be 0 mm, the axial coordinate of swirler exit is 45 mm.).

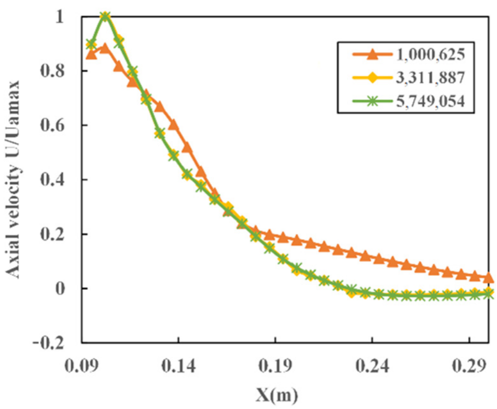

Figure 3. Axial velocity on central axis in cases of different grid numbers.

In order to ensure the reliability of the numerical simulation, Scheme S1 was selected for comparative verification of the experimental and simulation results under the typical condition. The PIV [18] optical diagnostic platform was adopted to obtain the flow field of the combustor under the condition of 3% pressure drop. Three-dimensional numerical simulation of Scheme S1 was carried out at the same operating condition. Comparison between experimental and numerical results of axial velocity at different locations is shown in Figure 4. Where U/U_{max} represents the normalized axial velocity, d represents the axial distance between the selected plane and the exit plane of the swirler. Figure 4 shows that the numerical simulation results are basically consistent with the PIV experimental results, which proves that the numerical method with this model could be applied to predict the flow field characteristics.

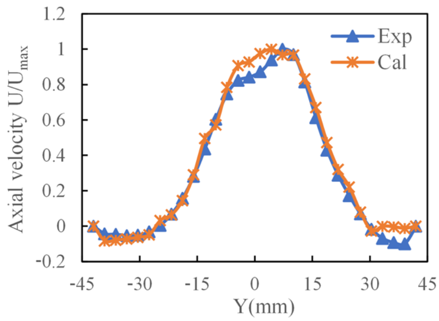

(**a**) Radial profile of axial velocity at d = 20 mm

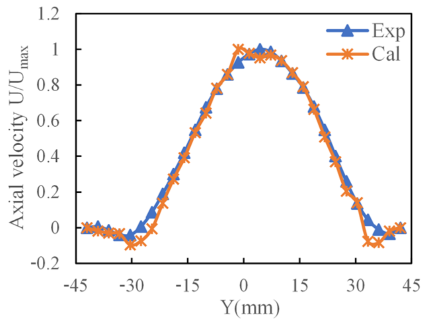

(**b**) Radial profile of axial velocity at d = 30 mm

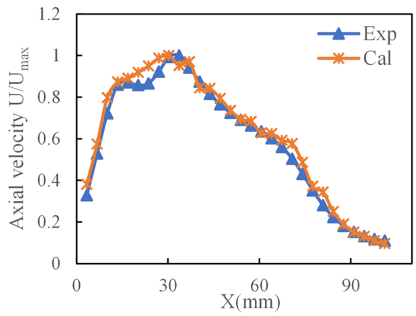

(**c**) Axial profile of axial velocity on the central line

Figure 4. Comparison between numerical and experimental results of axial velocity.

3. Results and Discussion

3.1. Effect of Inner Swirler Parameters on Flow Field

Figure 5 shows the effect of internal swirl parameters on the flow filed in Schemes S1–S4, the black line at the bottom half of the flow filed is an isoline with zero axial velocity. It could be seen that when the outer swirl number (SN_o) is fixed at 0.695, the Primary Recirculation Zone (PRZ) is gradually formed with the increase in the inner swirl number (SN_i). The vortex center of PRZ gradually approaches the downstream and radially outer sides of the combustion chamber, and the axial velocity at the downstream decreases gradually. As shown in Figure 5a, when SN_i is 0.235, the airflow near the swirler outlet flows downstream directly. In this condition, the PRZ is not formed, but two Corner Recirculation Zones (CRZ) are formed near the wall of the combustor. The vortex center positions of CRZ are (57 mm, 36 mm) and (100 mm, 33 mm), respectively. However, as illustrated in Figure 5b, as SN_i increases from 0.235 to 0.266, there is a distinct angle of the airflow at X = 90 mm near the centerline. Affected by the airflow radially expanding, the two corner vortices merge into one, and the vortex center is (78 mm, 35 mm). No PRZ is formed in this condition as well. The PRZ is formed as the SN_i increases from 0.235 to 0.402, as shown in Figure 5c. The starting position of PRZ is X = 52 mm and vortex center is (115 mm, 30 mm). Meanwhile, the axial velocity downstream of swirler is greatly reduced. However, with SN_i increasing from 0.402 to 0.427, as illustrated in Figure 5d, the axial velocity at the swirler outlet decreases slightly. The starting position of PRZ is X = 52 mm and the coordinate of vortex center is (127 mm, 35 mm). The axial length of the PRZ is 108 mm.

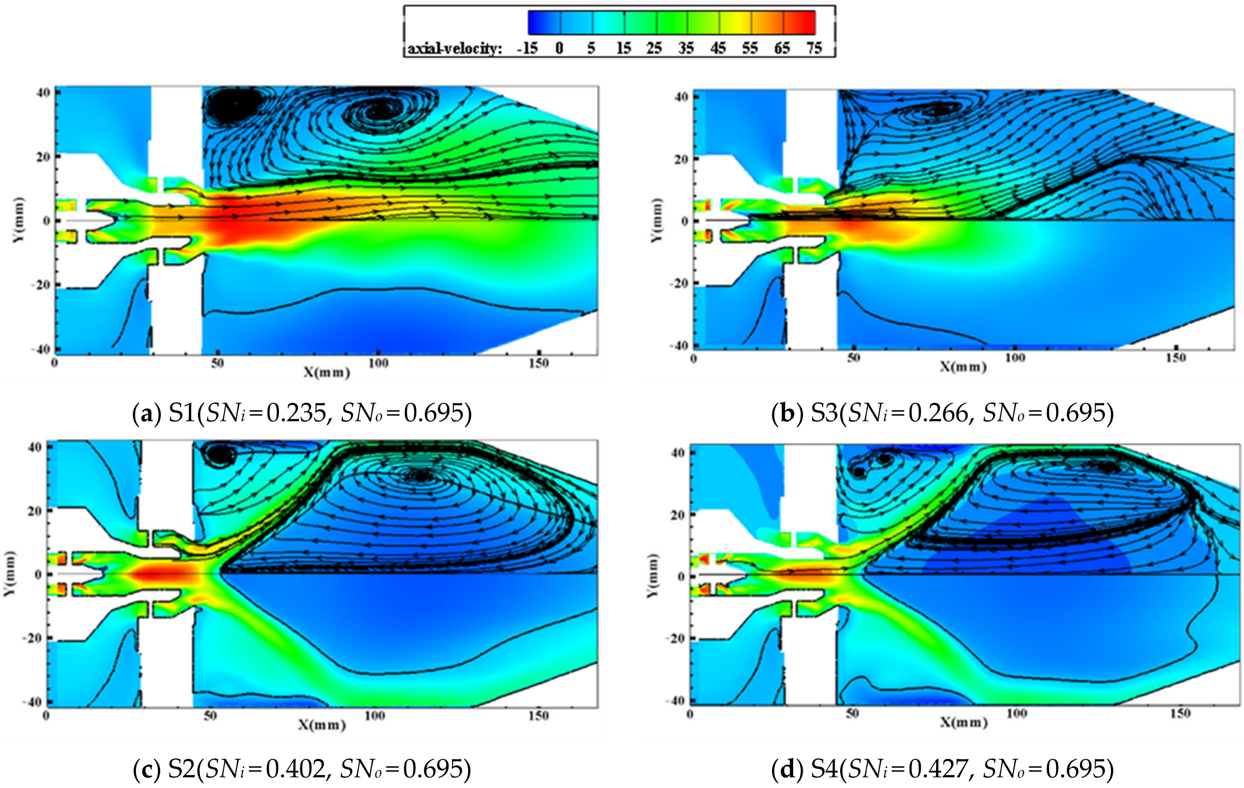

Figure 5. Axial velocity contour and streamline of Scheme S1–S4.

Figure 6 shows the comparison between the PRZ shape of Schemes S2 and S4. It could be seen that the starting position and expansion angle of the PRZ of these two Schemes are basically the same. As the air flows downstream, the radial width of the PRZ increases first and then decreases. Compared with Scheme S4, the PRZ size of Scheme S2 is longer and narrower. The flow topology of Scheme S4 is better than Scheme S2 because the shorter PRZ length of Scheme S4 helps to reduce the length of combustor.

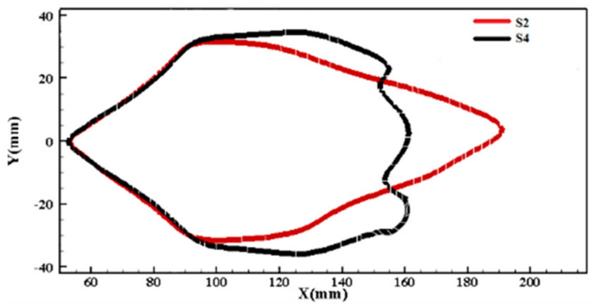

Figure 6. Comparison between the PRZ of Schemes S2 and S4.

Figures 7–9 show the comparison of different velocity components between Schemes S1 to S4, including axial velocity, radial velocity and tangential velocity at different planes.

The velocity dimension at 2 mm downstream of swirler exit is large. As is shown in Figure 7a, the peak values of axial velocity of Schemes S1–S4 are concentrated near the central axis of combustor. Among these schemes, the highest axial velocity could reach 70 m/s in Scheme S3; the reason is that the smaller blade angle of Scheme S3 leads to a stronger axial momentum of the airflow. In terms of radial velocity, compared with Schemes S1 and S3, the radial velocities near the wall of Schemes S2 and S4 are lower (see Figure 8a). However, near the central axis, the radial velocities of Schemes S2 and S4 are higher. Meanwhile, the radial velocities at radially outside of swirler of Schemes S2 and S4 are mostly negative, which means that the air flows inward along the radial direction in these two schemes. For the tangential velocity, as is shown in Figure 9a, with the increase in SN_i, the tangential velocity increases near the center axis at plane of d = 2 mm.

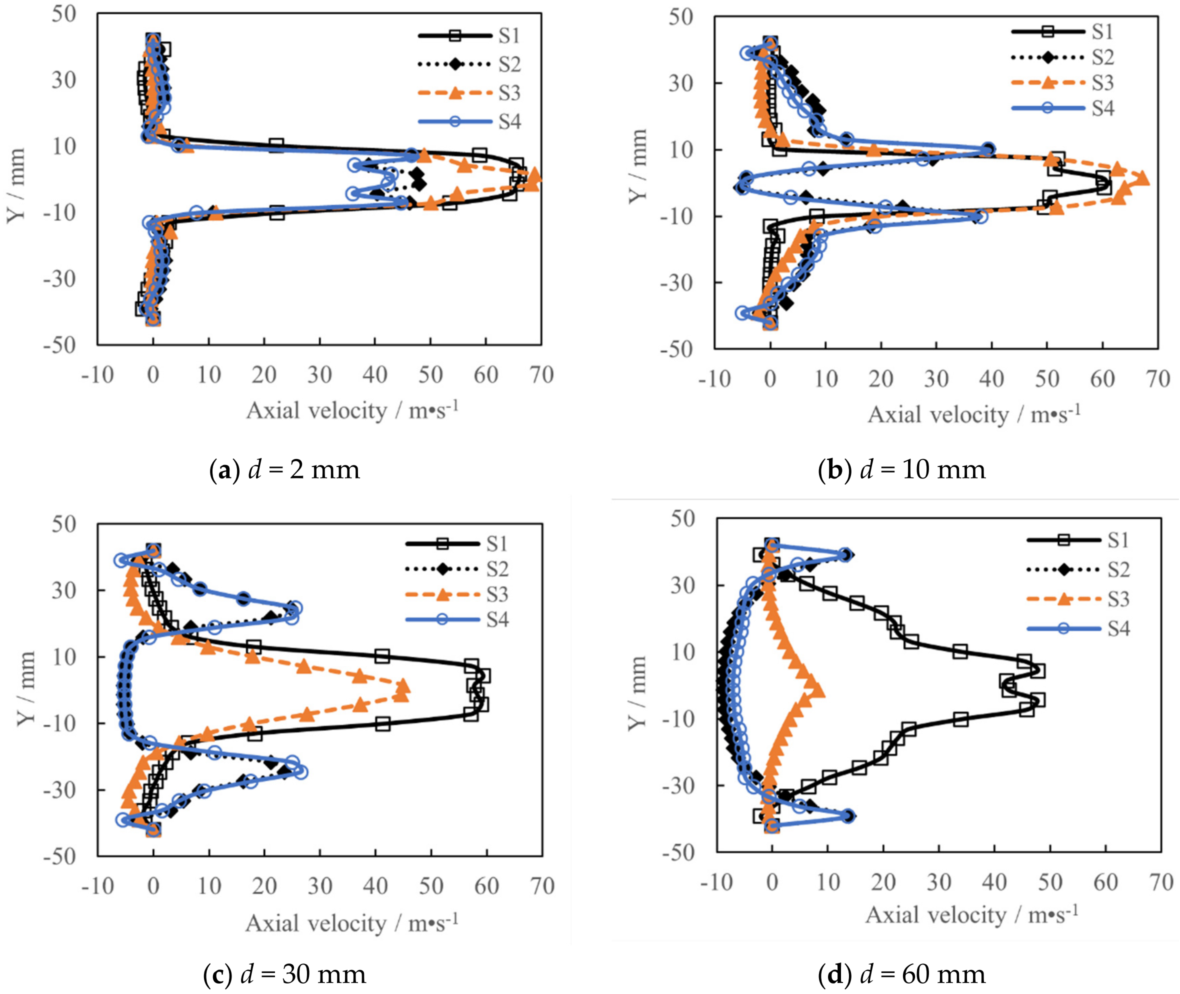

Figure 7. Radial profile of axial velocity at different axial sections.

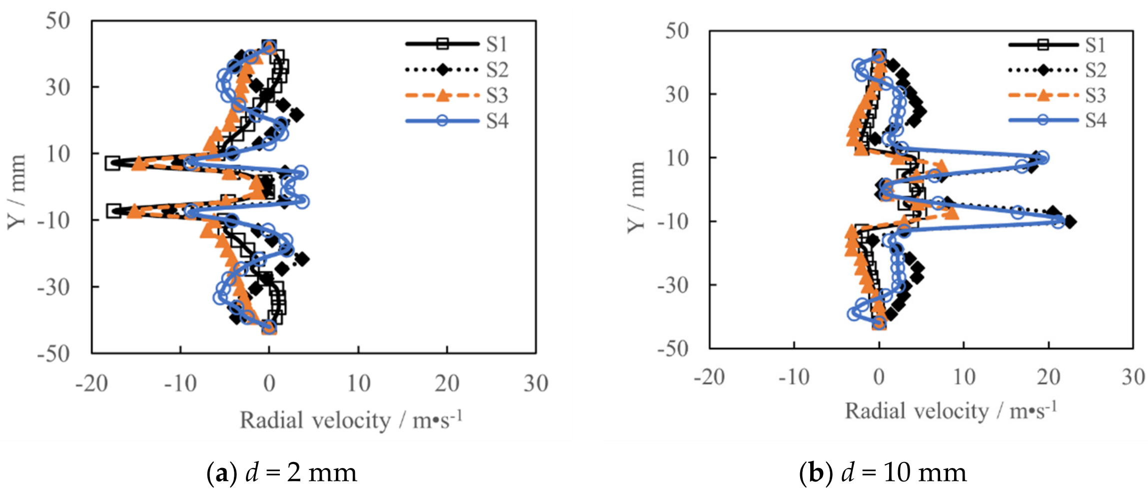

Figure 8. *Cont.*

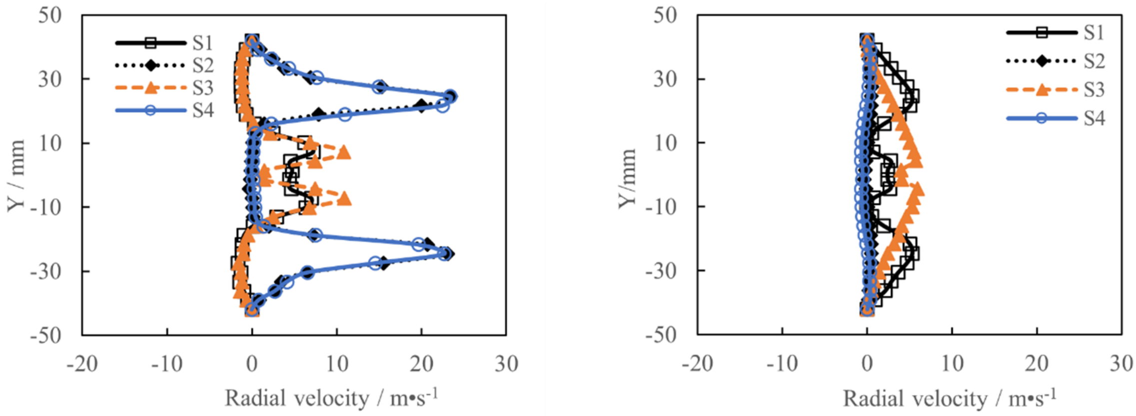

(**c**) *d* = 30 mm (**d**) *d* = 60 mm

Figure 8. Radial profile of radial velocity at different axial sections.

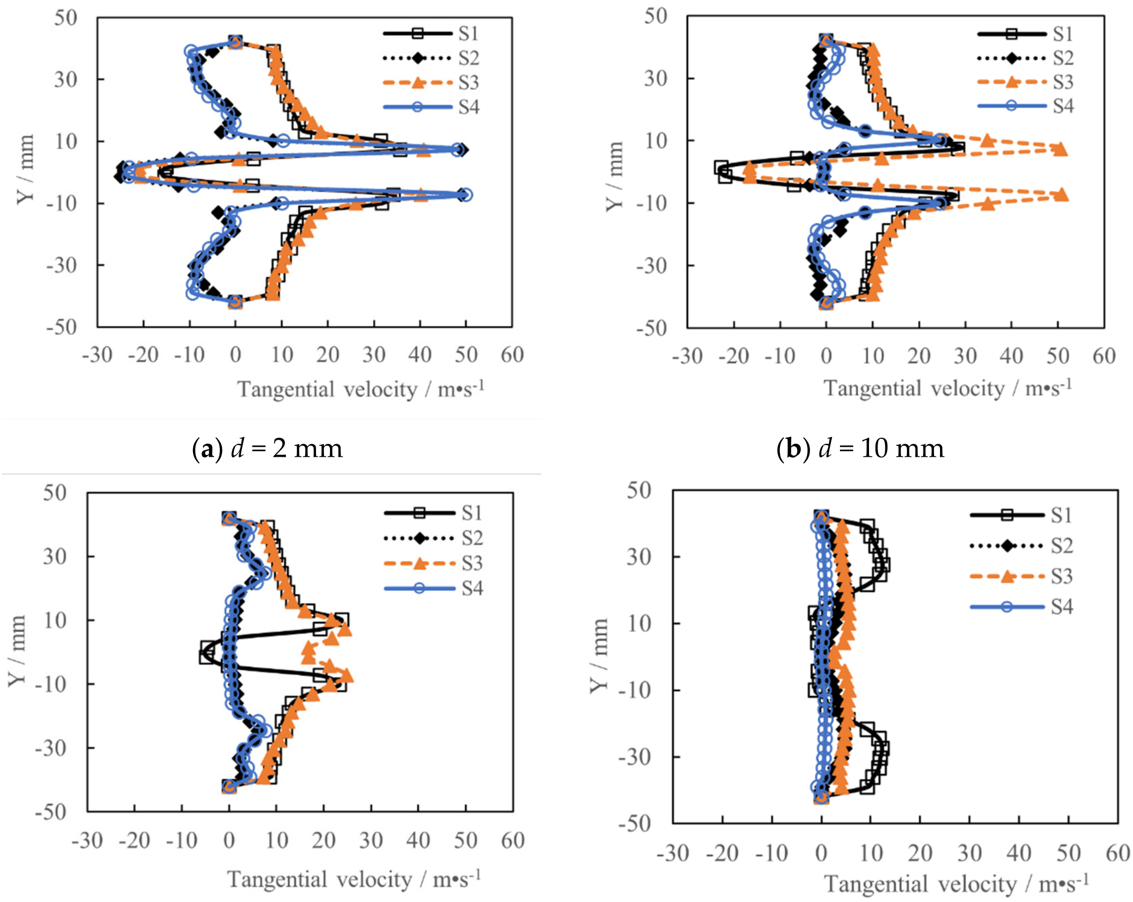

(**a**) *d* = 2 mm (**b**) *d* = 10 mm

(**c**) *d* = 30 mm (**d**) *d* = 60 mm

Figure 9. Radial profile of tangential velocity at different axial sections.

At 10 mm downstream of the swirler exit, as illustrated in Figure 7b, the negative axial velocity regions are observed on the central axis of Schemes S2 and S4, which proved that the PRZ are formed in the flow field. Compared with Schemes S1 and S3, the tangential velocities of Schemes S2 and S4 are significantly reduced and the radial velocities are significantly increased, see Figures 8b and 9b. This indicates that part of tangential velocity converts into radial velocity, which forms a central low-pressure zone, thus promoting the formation of PRZ.

At 30 mm downstream of the exit, as shown in Figure 7b,c, the radial widths of the PRZ increase under Schemes S2 and S4 compared with 10 mm downstream of swirler exit.

At 60 mm downstream, the radial width of the PRZ under Schemes S2 and S4 continues to increase (see Figure 7d). In addition, a negative axial velocity region is formed in Scheme S4, resulting in a narrow PRZ. In terms of the tangential velocity, compared with Scheme S2, the tangential velocity of Scheme S4 decreases and the inverse pressure gradient decreases at this location (see Figure 9d).

The developments of each velocity component near the swirler exit are summarized in Figure 10. As is illustrated in Figure 10c,d, the radial velocities of Schemes S2 and S4 (in which the PRZ have formed) raise along the central axis in proximity of the exit. Moreover, both the tangential velocities of outer-swirl flow and that of inner-swirl flow decrease. However, the tangential velocity of outer-swirl flow drops more rapidly than the inner-swirl tangential velocity. We infer that part of the outer-swirl tangential velocity counteracts the inner-swirl tangential velocity, and the other part of the outer-swirl tangential velocity converts to the radial velocity of main flow. This leads to an increasing trend of radial velocity of main flow, as is indicated in Figure 10 c,d. The increase in radial velocity results in a trend that sees the airstream flow more easily away from the central axis, forming a local low-pressure zone. This local low-pressure zone sucks the air from the downstream, resulting in the formation of the PRZ. Thus, we conclude that it is the transition of tangential velocity to radial velocity that promotes the formation of the PRZ.

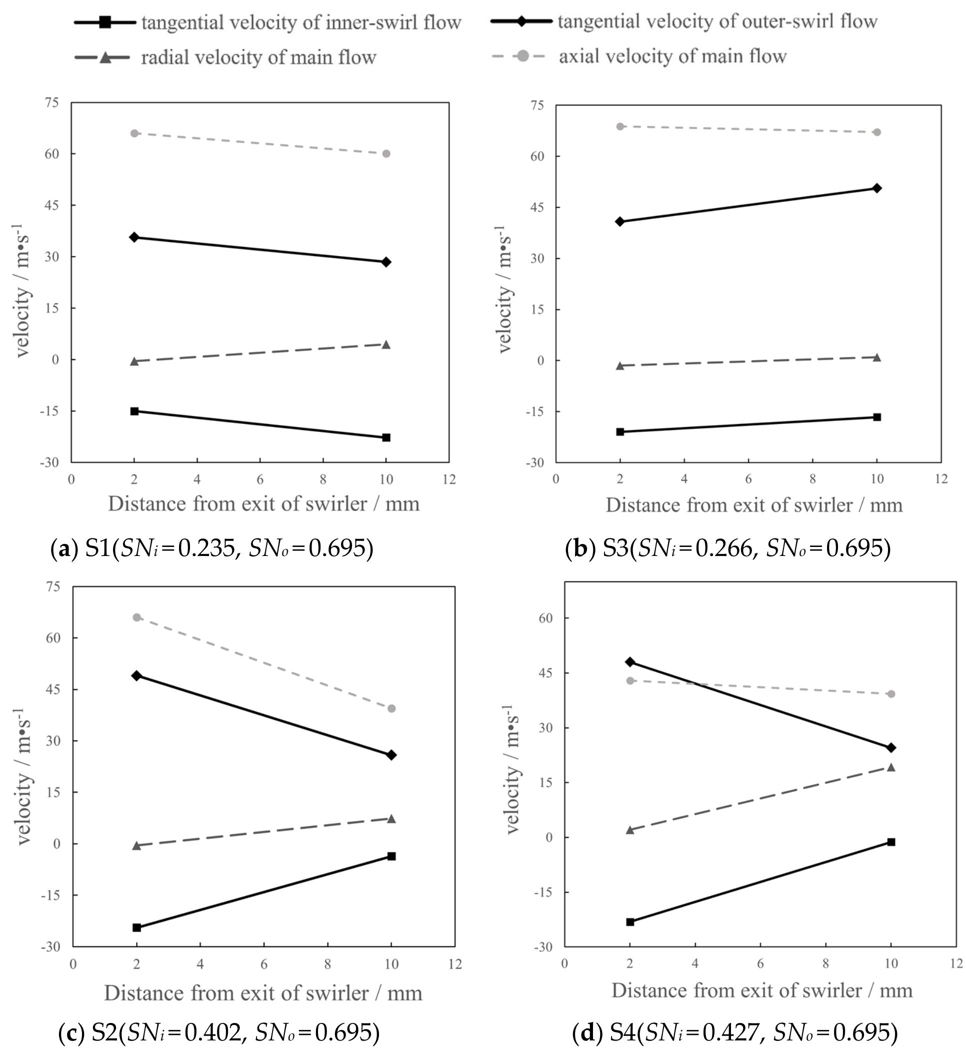

Figure 10. Summary of the development of each velocity component near the swirler exit.

Figure 11 shows the radial profiles of turbulent kinetic energy at d = 2 mm of Schemes S1–S4. It could be seen that the distribution trend of turbulent kinetic energy at d = 2 mm is basically consistent at different inner swirl numbers. With the increase in SN_i, the turbulent kinetic energy decreases at the center axis of the swirler outlet and increases at the outer swirler exit. This indicates that the shear effect between internal and external flow increases with the increase in internal swirl intensity, and the momentum dissipation in the shear layer leads to the increase in turbulence intensity.

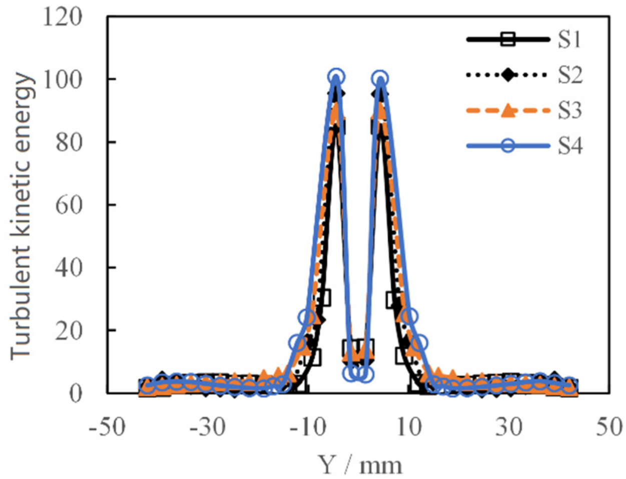

Figure 11. Radial profiles of turbulent kinetic energy at d = 2 mm under Schemes S1–S4.

3.2. Effect of Outer Swirler Parameters on Flow Field

We have already discussed the effect of inner swirler structural parameters on the flow topology, by altering the installation angle and number of blades of inner swirler. In this section, we will focus on analyzing the flow filed with variations of outer swirler structural parameters.

Figure 12 shows the flow filed of the Schemes S5 and S6 (which represents the effect of blade installation angle of outer swirler). The black line at the bottom half of the figure is an isoline with zero axial velocity. Figure 13 illustrates the shape of the PRZ of Schemes S5 and S6. Combined with Figure 5a (Scheme S1), it can be observed that, keeping the inner swirl number SN_i at 0.235, the PRZ is gradually formed and the starting position of PRZ moves forward with the increase in the SN_o. As SN_o increases from 0.695 to 0.987, there is a distinct angle of airflow at the exit of swirler; this angle is more pronounced at the inner swirler exit. The PRZ is formed at 4 mm downstream of the swirler outlet, and the vortex center of PRZ is (123 mm, 26 mm). The axial length of PRZ extends to the combustor outlet. Furthermore, as SN_o increases from 0.987 to 1.434, the PRZ is formed at 2.5 mm downstream of the swirler outlet, which is earlier compared with Scheme S5. Moreover, the vortex center moves forward to (119 mm, 32 mm). The axial length of the PRZ shrinks to 120.5 mm with a larger angle of swirling jet flow.

Figures 14–16 show the radial distribution of axial velocity, radial velocity and tangential velocity in planes at different distances from the swirler exit under Schemes S1, S5 and S6.

At 2 mm downstream of swirler exit, it is noticed in Figures 14a and 15a that the axial velocity at the central axis gradually decreases with the increase in SN_o and the radial velocity gradually increases from negative to positive. This elucidates that the increase in SN_o alters the airflow direction at the swirler exit. Moreover, the larger SN_o is, the more obvious is the increase in radial velocity. In addition, the radial velocity of Scheme S6 increases more significantly and the PRZ is formed more upstream compared with Scheme S5 (see Figure 15a). This phenomenon indicates that the earlier the tangential velocity is converted to radial velocity at the swirl exit, the easier the PRZ is formed.

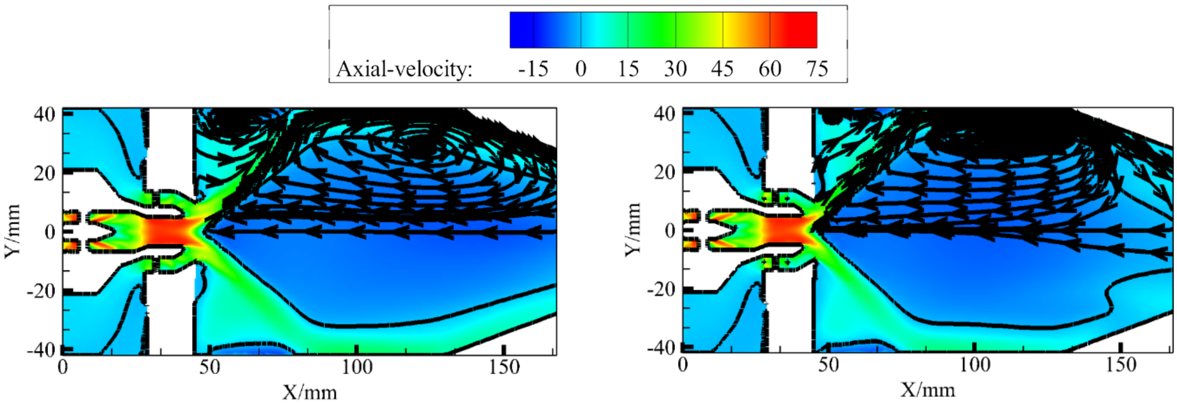

(**a**) S5($SN_i = 0.235$, $SN_o = 0.987$) (**b**) S6($SN_i = 0.235$, $SN_o = 1.434$)

Figure 12. Effect of outer-stage swirl parameters on the flow field.

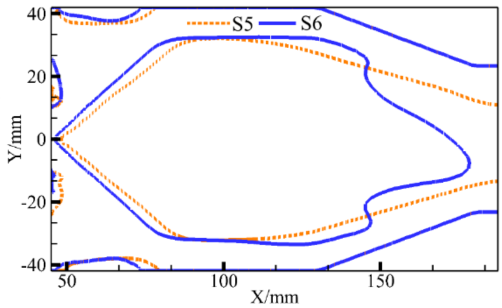

Figure 13. The shape of PRZ under Schemes S5 and S6.

It is noticed that at 10 mm downstream of swirler exit, the axial velocity and tangential velocity at central axis decrease further, while the radial velocity continues to increase, as indicated in Figures 14b, 15b and 16b. The negative axial velocity region is observed near the central axis in Schemes S5 and S6, indicating that there is a PRZ in the flow field (see Figure 14b). Moreover, the radial width of the PRZ increases with the increase in SN_o, which demonstrates that stronger SN_o results in a faster dissipation of the tangential momentum.

Figure 14c illustrates that at 30 mm downstream of swirler exit, the radial width of the PRZ continues to increase with the increase in SN_o. As indicated in Figure 15c, compared with Schemes S1 and S6, the attenuation of radial momentum decreases under Scheme S5 at 30 mm downstream.

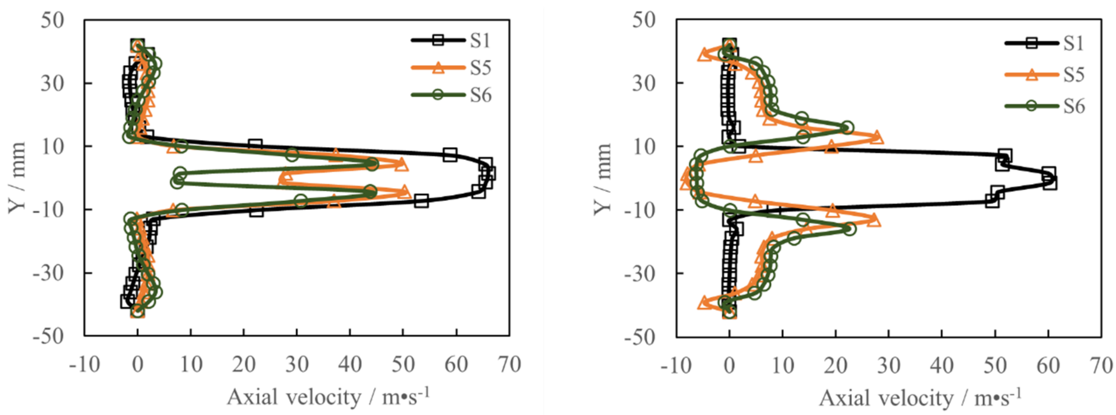

(**a**) $d = 2$ mm (**b**) $d = 10$ mm

Figure 14. *Cont.*

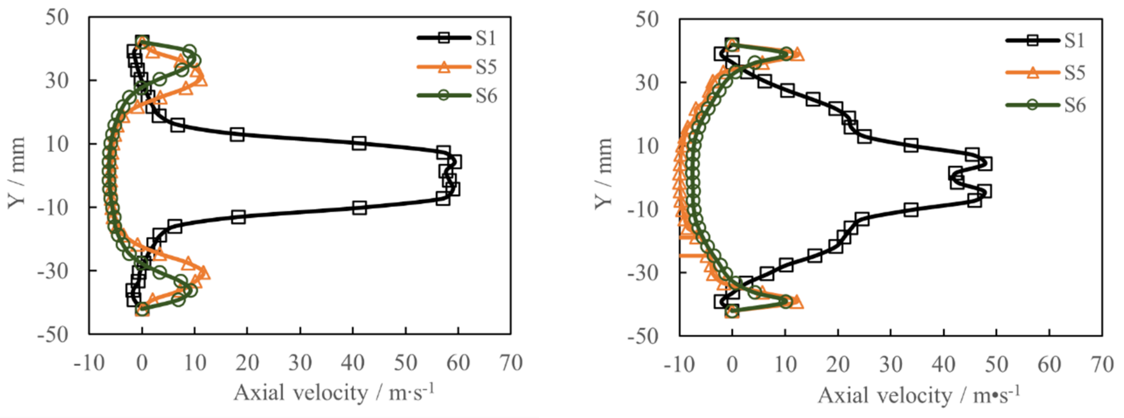

(c) d = 30 mm (d) d = 60 mm

Figure 14. Radial profiles of axial velocity.

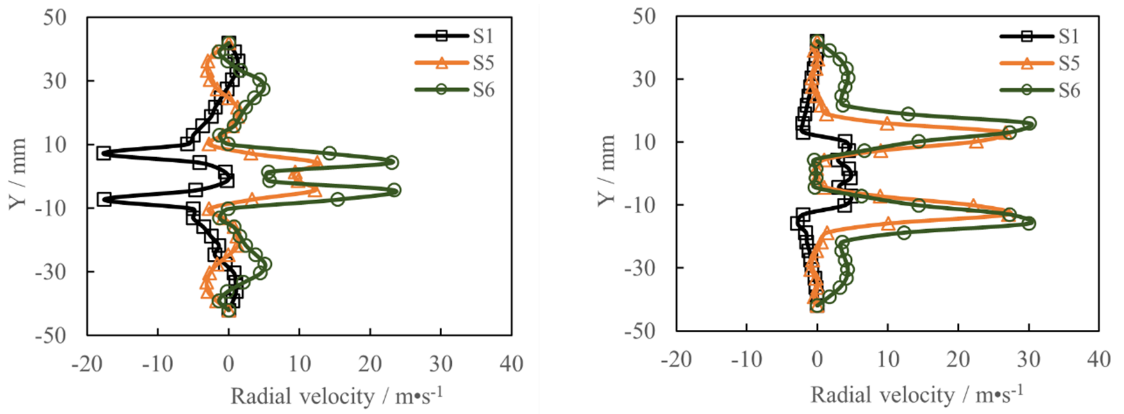

(a) d = 2 mm (b) d = 10 mm

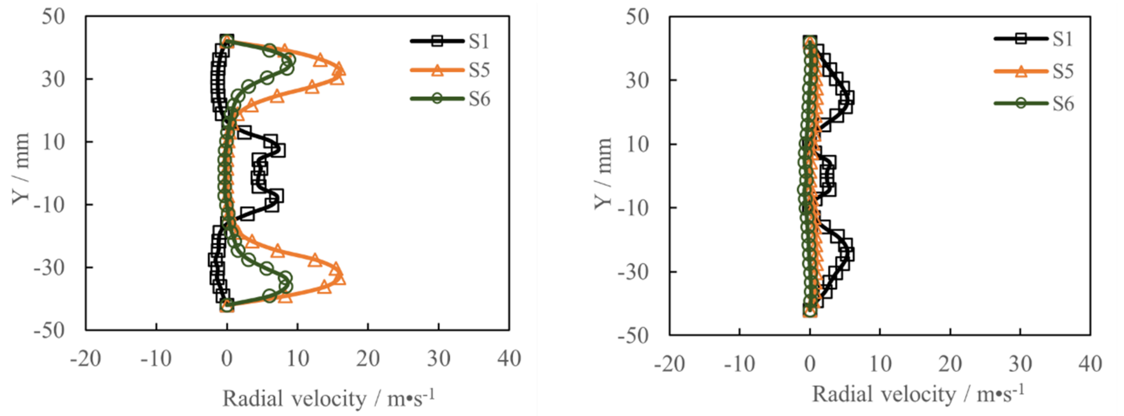

(c) d = 30 mm (d) d = 60 mm

Figure 15. Radial profiles of radial velocity.

Figure 14d indicates that at 60 mm downstream of swirler outlet, the negative axial velocity at the central axis of Scheme S5 increases, compared with that at d = 30 mm.

We infer that the reason why the radial velocity at 2 mm downstream of exit increases from negative (Scheme S1) to positive (Schemes S5 and S6) with the increase in SN_o is that a high positive tangential velocity dissipates the negative radial velocity in Scheme S5 and S6 (see Figure 16a). After that, the rest of the tangential velocity transforms to positive radial velocity to support airstream flows toward the wall and then flows downstream, forming a relatively long and narrow PRZ. Thus, it can be inferred that the increase in SN_o makes the tangential velocity at the exit of the external swirler rapidly transform to the radial velocity, which changes the direction of the airflow at the swirler exit. This change makes the outer swirling air have a tendency to diffuse away from the center of combustor, forming a central low-pressure zone. The reverse flow formed in this way induces the airflow at the outer swirler exit to transform from tangential flow to radial flow, further promoting the formation of the PRZ. To some extent, this also indicates that the strong swirling flow is the main factor influencing the flow field structure of the swirler.

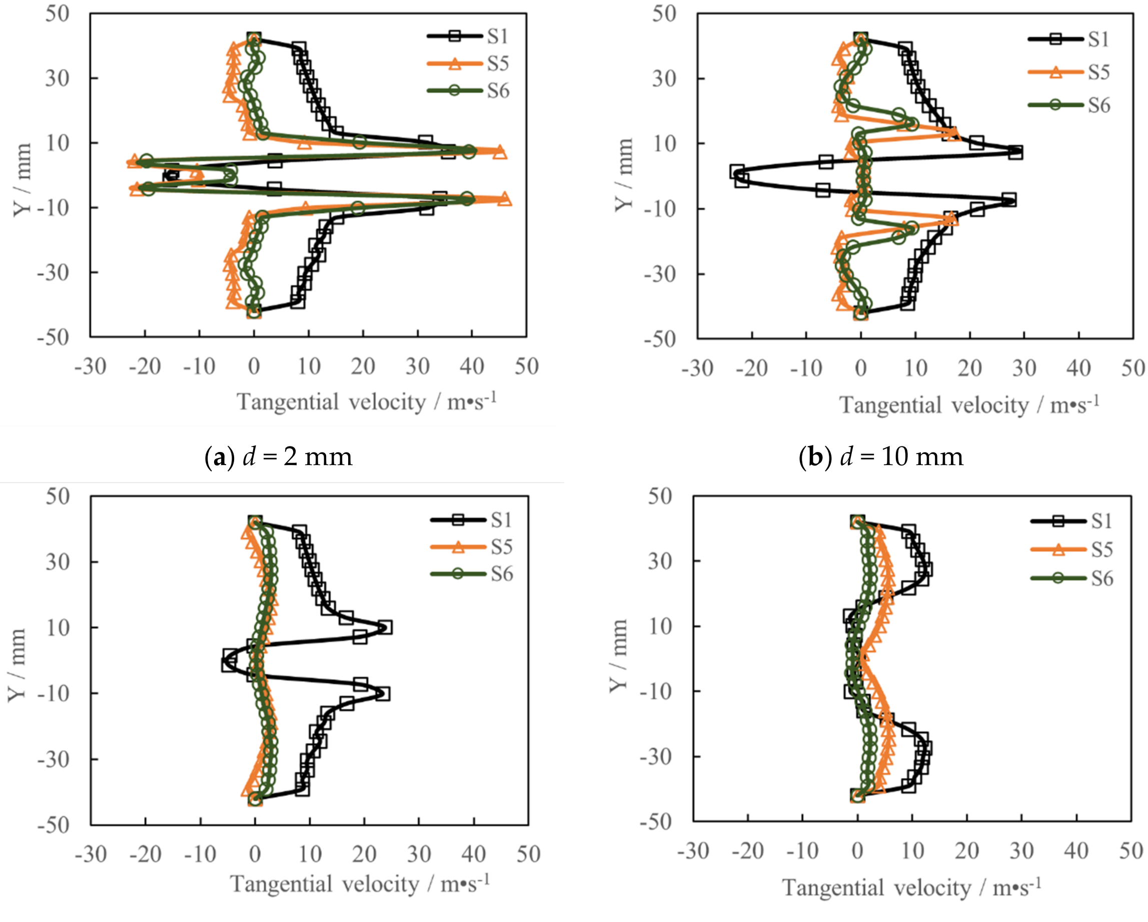

(**a**) *d* = 2 mm (**b**) *d* = 10 mm (**c**) *d* = 30 mm (**d**) *d* = 60 mm

Figure 16. Radial profiles of tangential velocity.

3.3. Effect of Sleeve Angles on Flow Field

In this section, we will discuss the effect of the sleeve angles of outer swirler on flow topology. Schemes S1 and S7 with sleeve angles of 30° and 15° were selected to carry out the numerical simulation of the flow filed. The obtained axial velocity contours and streamlines are shown in Figure 17. And the tangential velocity contours are shown in Figure 18. It is noticed from Figure 17 that, as the sleeve angle changes from β = 30° to β = 15°, the flow field transforms from CRZ-dominated to PRZ-dominated. In the scheme of β = 15°, the starting position of the PRZ is 15 mm from swirler exit, and the coordinate of vortex center is (96 mm, 26 mm). Moreover, in the scheme of β = 30°, the larger sleeve angle makes the swirling air of the outer stage directly flow along the axis, without distinct diffusion angle. The reason for this phenomenon is that the outer stage airflow suppresses the inner-stage airflow flow along radially outer direction, which makes the inner-stage swirling air converges to the central axis, and the high-speed region is concentrated in the center of the combustor.

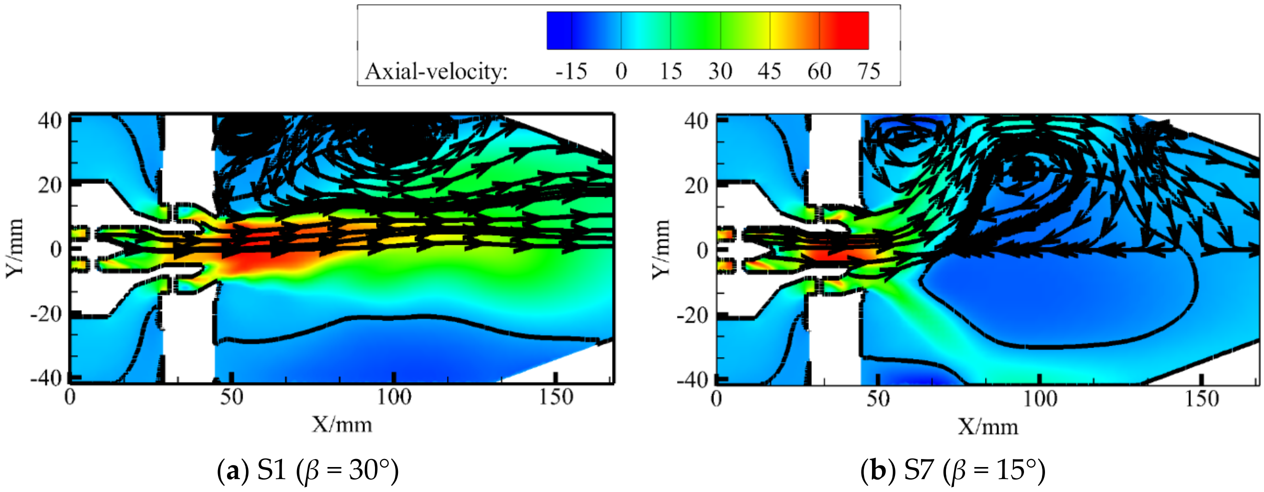

Figure 17. Axial velocities contours and streamline under different sleeve angles.

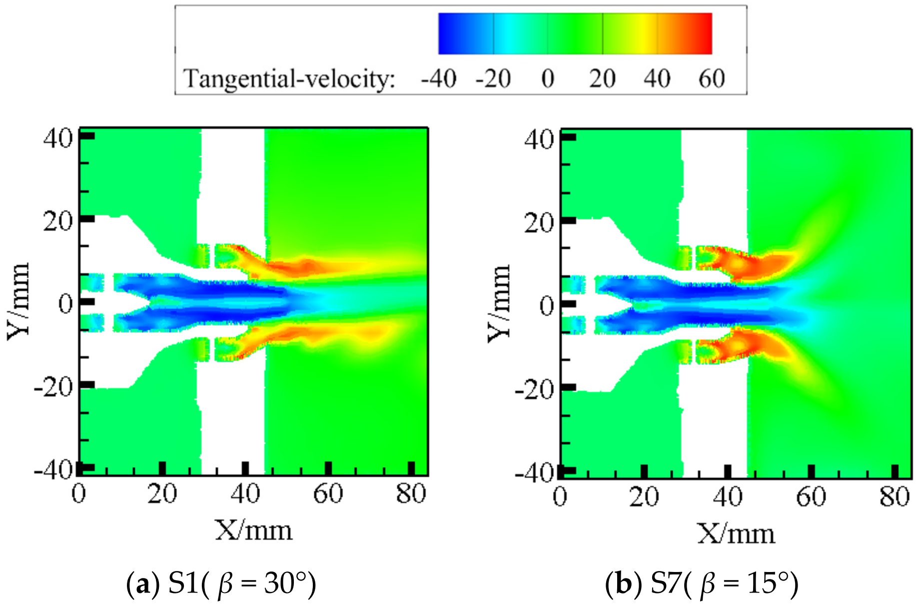

Figure 18. Tangential velocities contours under different sleeve angles.

Figures 19–21 show the radial distribution of axial velocity, radial velocity and tangential velocity in planes at different distances from the swirler exit under Schemes S1 and S7.

The radial velocity at 2 mm downstream of the outer swirler exit with β = 15° is larger than that of the scheme of β = 30°, as shown in Figure 20a. This indicates that the dissipation effect between the internal and external counter-rotated swirling air is weakened, and part of the tangential velocity is converted to the radial velocity, which is conducive to the formation of the PRZ.

Then, at 10 mm downstream from the exit, with the increase in distance from swirler exit, the axial velocity and tangential velocity of Scheme S7 decrease significantly, while radial velocity of Scheme S7 increases obviously (see Figures 19b, 20b and 21b).

At 30 mm downstream of the swirler exit, the negative axial velocity region is observed near the central axis, and the PRZ is formed, as shown in Figure 19c. As the swirling airstream flows downstream, part of tangential momentum is dissipated, and part of it is converted into radial momentum, leading the airstream flow radially outward. This promotes the formation of PRZ.

From Figure 17, we notice that the radial width of the PRZ increases significantly at 60 mm downstream in Scheme S7 with β = 15°. The airflow recirculation is obvious.

In conclusion, compared with altering the swirl number, the PRZ obtained by changing the sleeve angle is more downstream in the combustor, and the size of the PRZ is significantly reduced.

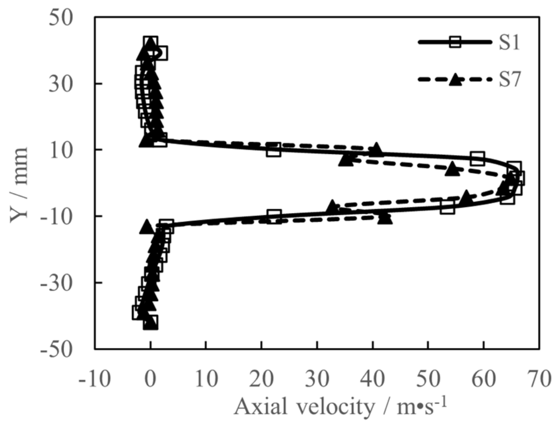

(**a**) *d* = 2 mm

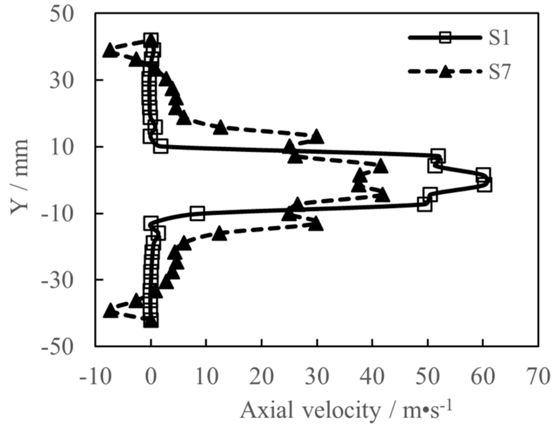

(**b**) *d* = 10 mm

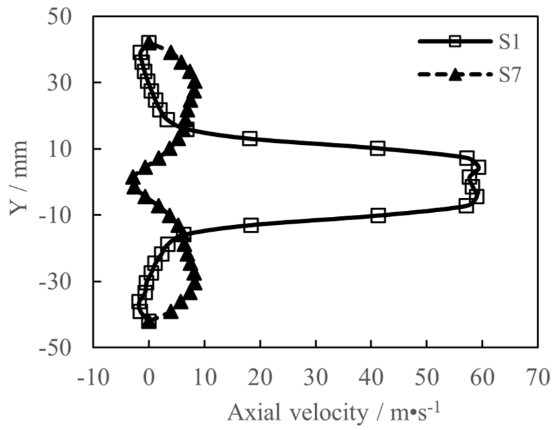

(**c**) *d* = 30 mm

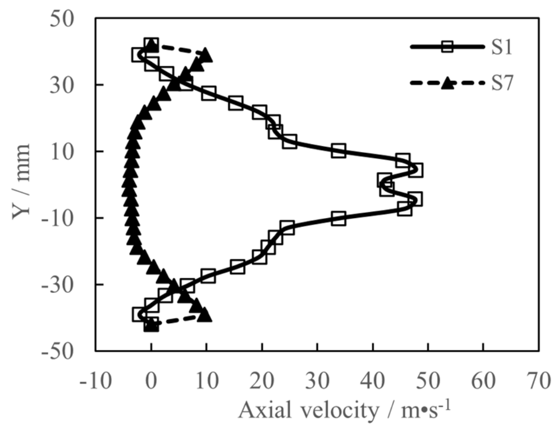

(**d**) *d* = 60 mm

Figure 19. Radial profiles of axial velocity.

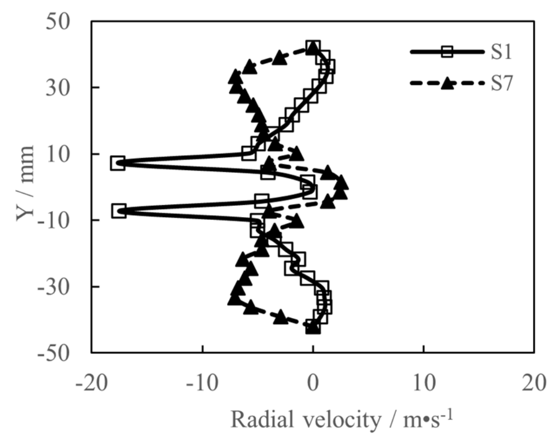

(**a**) *d* = 2 mm

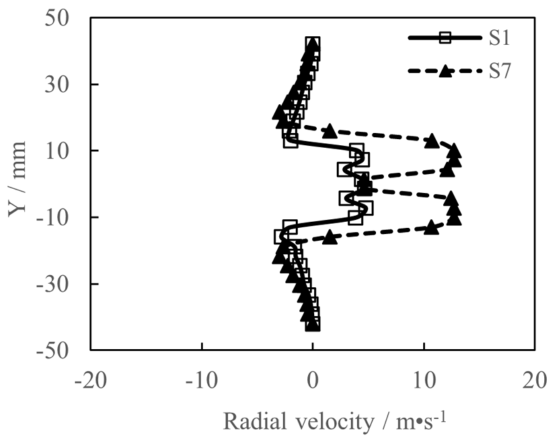

(**b**) *d* = 10 mm

Figure 20. *Cont.*

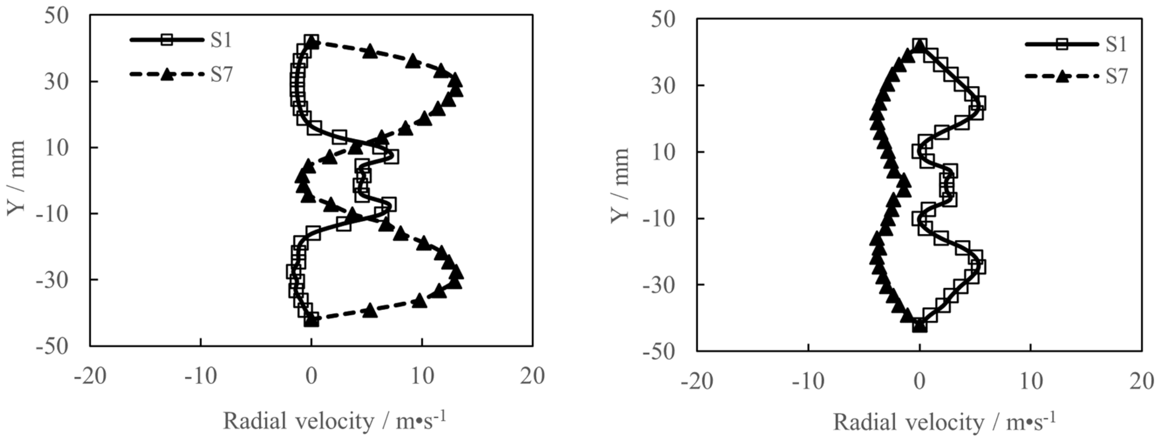

(**c**) *d* = 30 mm (**d**) *d* = 60 mm

Figure 20. Radial profiles of radial velocity.

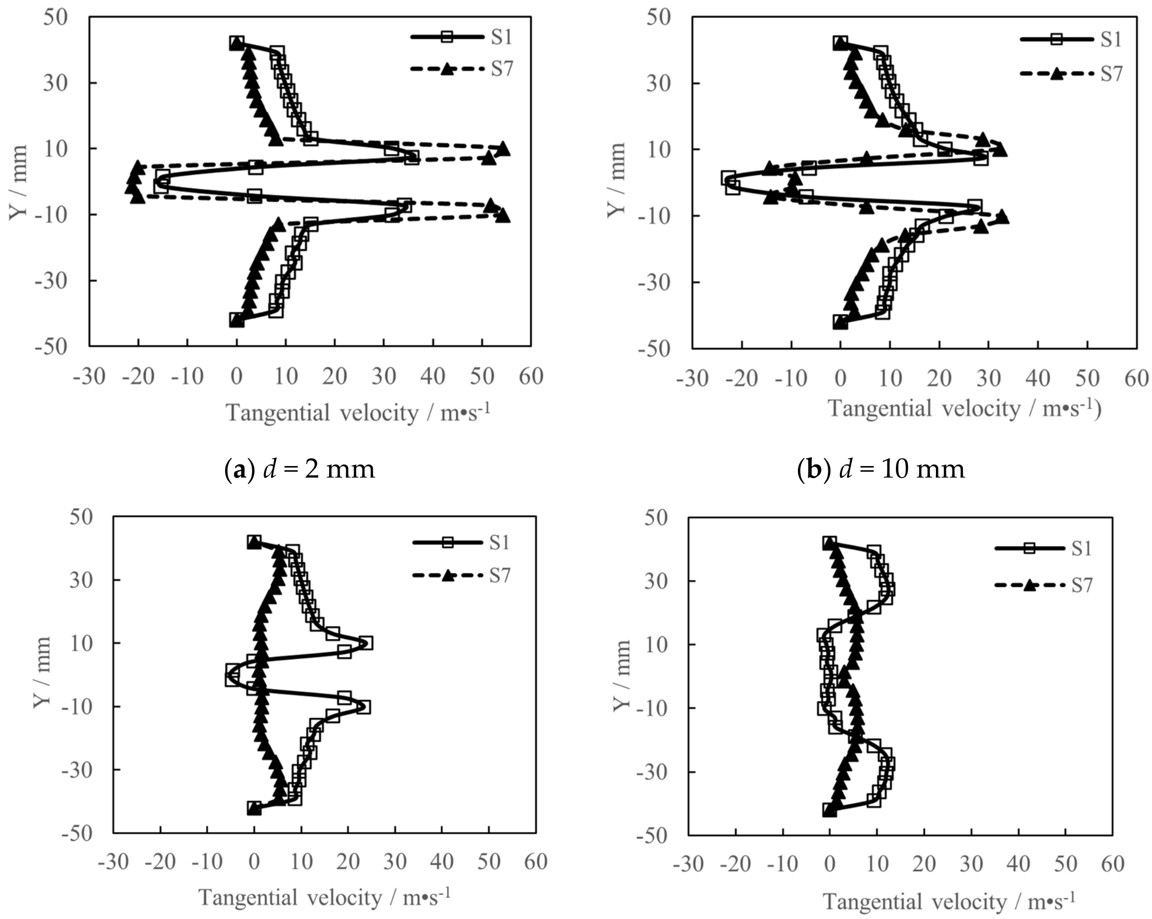

(**a**) *d* = 2 mm (**b**) *d* = 10 mm

(**c**) *d* = 30 mm (**d**) *d* = 60 mm

Figure 21. Radial profiles of tangential velocity.

4. Conclusions

In this work, three-dimensional numerical simulation of the flow field under different key structural parameters of the prefilming air-blast fuel injector was carried out. The influence of the key structural parameters on the flow field is explored, and the development of the two-stage swirling air in the combustor and the mechanism of coupling effect of these two counter-rotating airflows were analyzed, which provides support for the regulation and optimization of flow field in the swirl combustor. The main conclusions are as follows:

It is the transition of tangential velocity of airflow to radial velocity in swirling airflow that promotes the formation of the PRZ. The shearing interaction between inner- and outer-counter-rotational swirling airflows is strengthened with the increase in SN_i. This changes the transition process of the velocity components and flow trajectory of the outer-stage swirling air. By increasing SN_o, the transition process from tangential momentum to radial momentum is accelerated, which is also helpful for the formation of PRZ. The decrease in sleeve angle β and the increase in swirl number share a similar mechanism on influencing the formation of PRZ; both of them bring about the transition process of the velocity component and flow trajectory variation of the outer-stage swirl in the combustor. However, the difference is that the axial length and radial width of the PRZ formed by decreasing β are smaller and more downstream than by increasing swirl number.

Author Contributions: Funding acquisition, G.X.; Investigation, C.C.; Methodology, Y.G. and F.L.; Project administration, C.L. and G.X.; Supervision, C.L., Y.M. and D.M.; Validation, S.W.; Writing—original draft, C.C. and Y.G.; Writing—review & editing, C.L. All authors have read and agreed to the published version of the manuscript.

Funding: The present work is financially supported by the National Science and Technology Major Project (J2019-III-0005-0048 & 2017-III-0007-0032).

Data Availability Statement: The data presented in this study are available on request from the corresponding author. The data are not publicly available due to privacy issue.

Conflicts of Interest: The authors declare no conflict of interest.

References

1. Sovani, S.D.; Sojka, P.E.; Lefebvre, A.H. Effervescent Atomization. *Prog. Energy Combust. Sci.* **2001**, *27*, 483–521. [CrossRef]
2. Kim, J.Y.; Lee, S.Y. Dependence of Spraying Performance on the Internal Flow Pattern in Effervescent Atomizers. *At. Sprays* **2001**, *11*, 6.
3. Lin, K.-C.; Kennedy, P.; Jackson, T. Structures of Internal Flow and the Corresponding Spray for Aerated-Liquid Injectors. In Proceedings of the 37th Joint Propulsion Conference and Exhibit, Salt Lake City, UT, USA, 8–11 July 2001.
4. Catlin, C.A.; Swithenbank, J. Physical Processes Influencing Effervescent Atomizer Performance in the Slug and Annular Flow Regimes. *At. Sprays* **2001**, *11*, 5.
5. Durbin, M.D.; Ballal, D.R. Studies of Lean Blowout in a Step Swirl Combustor. *J. Eng. Gas Turbines Power* **1996**, *118*, 72–77. [CrossRef]
6. Wang, Z.; Jiang, C.; Xu, H.; Wyszynski, M.L. Macroscopic and Microscopic Characterization of Diesel Spray under Room Temperature and Low Temperature with Split Injection. *Fuel Process. Technol.* **2016**, *142*, 71–85. [CrossRef]
7. Kumar, S.; Malavalli, S.; Chaudhuri, S.; Basu, S. Spray Characteristics and Flow Topologies of High Shear Injector at High Primary Swirl. *Int. J. Multiph. Flow* **2020**, *131*, 103393. [CrossRef]
8. Lin, B.; Wu, Y.; Xu, M.; Chen, Z.-G. Experimental Investigation on Spark Ignition and Flame Propagation of Swirling Kerosene Spray Flames. *Fuel* **2021**, *303*, 121254. [CrossRef]
9. Davoudzadeh, F.; Liu, N.-S.; Moder, J.P. Investigation of Swirling Air Flows Generated by Axial Swirlers in a Flame Tube. In *Proceedings of the Volume 1: Combustion and Fuels, Education*; ASMEDC: Barcelona, Spain, 2006; pp. 891–902.
10. Zeng, Q.; Yuan, Y. Flow Dynamics of Dual-Stage Counter-Swirl Combustor in Different Confinement Spaces. *Int. Commun. Heat Mass Transf.* **2020**, *116*, 104633. [CrossRef]
11. Ren, X.; Brady, K.B.; Xue, X.; Sung, C.-J.; Mongia, H.C. Swirl Rotation Direction Effects on Lean Direct Injection Pilot Mixer Performance: Experiments and LES Modeling. *Aerosp. Sci. Technol.* **2022**, *129*, 107808. [CrossRef]
12. Mongia, H.; Al-Roub, M.; Danis, A.; Elliott-Lewis, D.; Johnson, A.; Vise, S.; Jeng, S.-M.; McDonell, V.; Samuelsen, G. Swirl Cup Modeling. I. In Proceedings of the 37th Joint Propulsion Conference and Exhibit, Salt Lake City, UT, USA, 8–11 July 2001; p. 3576.
13. Hsiao, G.; Mongia, H. Swirl Cup Modeling Part 2: Inlet Conditions. In Proceedings of the 41st Aerospace Sciences Meeting and Exhibit, Reno, NV, USA, 6–9 January 2003; p. 1350.
14. Hsiao, G.; Mongia, H. Swirl Cup Modeling Part 3: Grid Independent Solution with Different Turbulence Models. In Proceedings of the 41st Aerospace Sciences Meeting and Exhibit, Reno, NV, USA, 6–9 January 2003.
15. Youshida, K. Airblast Spray Characteristics of Planar Liquid Films in Longitudinal Gas-Phase Shear Layers at Various Ambient Pressure Conditions. In Proceedings of the 12th Triennial International Conference on Liquid Atomization and Spray Systems, Heidelberg, Germany, 2–6 September 2012.

16. Gupta, A.K.; Lilley, D.G.; Syred, N. Swirl Flows. *Tunbridge Wells* **1984**, *73*. Available online: https://ui.adsabs.harvard.edu/abs/1984tw...book.....G/abstract (accessed on 3 December 2022).
17. Syred, N.; Bekr, J.M. Combustion in Swirling Flows: A Review. *Combust. Flame* **1974**, *23*, 143–201. [CrossRef]
18. Yang, J.; Liu, C.; Liu, F.; Mu, Y.; Xu, G. Experimental and Numerical Study of the Effect of Main Stage Stratifier Length on Lean Blow-out Performance for a Stratified Partially Premixed Injector. *Proc. Inst. Mech. Eng. Part A J. Power Energy* **2018**, *232*, 812–825. [CrossRef]